Spectroscopic Comparison of the Heme Active Sites in WT KatG and Its S315T Mutant†

Gudrun S. Lukat-Rodgers,‡ Nancy L. Wengenack,§ Frank Rusnak,§ and Kenton R. Rodgers*,‡

Department of Chemistry, North Dakota State University, Fargo, North Dakota 58105 and Section of Hematology Research, Department of Biochemistry and Molecular Biology, Mayo Clinic, Rochester, Minnesota 55905

Received March 27, 2000; Revised Manuscript Received May 18, 2000

ABSTRACT: KatG, the catalase-peroxidase from *Mycobacterium tuberculosis*, has been characterized by resonance Raman, electron spin resonance, and visible spectroscopies. The mutant KatG(S315T), which is found in about 50% of isoniazid-resistant clinical isolates, is also spectroscopically characterized. The electron spin resonance spectrum of ferrous nitrosyl KatG is consistent with a proximal histidine ligand. The Fe-His stretching vibration observed at 244 cm^{-1} for ferrous wild-type KatG and KatG(S315T) confirms the imidazolate character of the proximal histidine in their five-coordinate high-spin complexes. The ferrous forms of wild-type KatG and KatG(S315T) are mixtures of six-coordinate low-spin and five-coordinate high-spin hemes. The optical and resonance Raman signatures of ferric wild-type KatG indicate that a majority of the heme exists in a five-coordinate high-spin state, but six-coordinate hemes are also present. At room temperature, more six-coordinate low-spin heme is observed in ferrous and ferric KatG(S315T) than in the WT enzyme. While the nature of the sixth ligand of LS ferric wild-type KatG is not completely clear, visible, resonance Raman, and electron spin resonance data of KatG(S315T) indicate that its sixth ligand is a neutral nitrogen donor. Possible effects of these differences on enzyme activity are discussed.

Mycobacterium tuberculosis (Mtb)[1] is the cause of 2−3 million human fatalities per year and is the second largest killer among infectious disease topped only by HIV/AIDS according to the latest World Health Organization report (*1*). This fatality rate, while striking, may worsen in light of emerging drug-resistant strains of *Mtb*. Recent outbreaks of drug-resistant strains of *Mtb* throughout the world (*2*, *3*) underscore the importance of understanding resistance at a level sufficient to support treatment development. The first line of defense against *Mtb* relies heavily on multiple antibiotics including the drug isoniazid (isonicotinic acid hydrazide, INH) (*4*−*6*). Although it is known that this antituberculosis drug inhibits mycolic acid synthesis in *Mtb* (*7*−*9*), its mechanism of action is not fully understood. Screening of INH-resistant isolates has revealed that the majority contain a point mutation in the *katG* locus (*10*−*13*), which encodes a heme-containing catalase-peroxidase (*14*). The most common mutation causing INH-resistant *Mtb* strains is KatG(S315T) (*11*, *15*, *16*). The drug sensitivity of these INH-resistant strains is restored upon introduction of a plasmid-borne functional *katG* (*17*, *18*), suggesting that INH is a prodrug that is activated by KatG.

Mtb and *Mycobacterium smegmatis* KatGs contain prosthetic protoheme centers and exhibit several enzymatic activities (*19*−*21*). Wild type (WT) *Mtb* KatG and KatG(S315T) proteins are both competent catalase-peroxidase enzymes (*22*, *23*). While peroxidase activity of KatG(S315T) is comparable to that of WT KatG, KatG(S315T) is less efficient at converting INH to isonicotonic acid via a mechanism involving superoxide as oxidant (*24*). The k_{cat} for INH oxidation catalyzed by KatG(S315T) is 7 times smaller than for WT KatG (*22*). Titration of ferric WT KatG with INH yields an absorbance difference spectrum that is not observed for the analogous titration of KatG(S315T) (*25*). The correlation between KatG(S315T) and *Mtb* resistance to INH represents an opportunity to probe the molecular basis of drug resistance in these *Mtb* strains.

Sequence alignment of KatG with cytochrome *c* peroxidase (CCP) suggests that Ser315 is part of the heme pocket in KatG (*11*, *14*). Therefore, differences in their heme electronic properties, heme environments, or bound INH orientations relative to the heme are possible explanations for the varying INH activation abilities reported for these two KatG proteins. However, ^{1}H- and ^{15}N-NMR relaxation measurements indicate that INH binds at approximately the same distance from the heme iron in both WT and KatG(S315T) (*25*, *26*), suggesting that the INH-binding site in KatG(S315T) is intact. Indeed, INH is able to competitively

† This work supported by NIH Grant AI41217-01 (to G.S.L.-R.), USDA Grant 96-35305-3628 (to K.R.R.), Hermann Frash Foundation Grant 446-HF97 (to K.R.R.), and the Mayo Foundation (to F.R.).

* To whom correspondence should be addressed. Telephone: (701) 231-8746. Fax: (701) 231-8831. E-mail: rodgers@plains.nodak.edu.

‡ North Dakota State University.

§ Mayo Clinic.

[1] Abbreviations: *Mtb*, *Mycobacterium tuberculosis*; WT, wild type; 6-c, six coordinate; 5-c, five coordinate; LS, low spin; HS, high spin rR, resonance Raman; ESR, electron spin resonance; INH, isonicotinic acid hydrazide; CCP, cytochrome *c* peroxidase; MnP, manganese peroxidase; CIP, *Coprinus cinereus* peroxidase; APX, pea cytosolic ascorbate peroxidase; HRP-C, horseradish peroxidase isoenzyme C; LPO, lactoperoxidase; SBP, soybean peroxidase; TP, turnip peroxidase; IP, intestinal peroxidase; JRP, Japanese horseradish peroxidase; Mb, myoglobin; HbA, hemoglobin A.

10.1021/bi0006870 CCC: $19.00
Published on Web 07/19/2000

inhibit KatG(S315T) with a K_I comparable to that of WT (*25*).

In this study, we present the first resonance Raman (rR) characterization of the ferric and ferrous forms of WT KatG. Elucidation of its spectral features will be used to ascertain which properties KatG has in common with CCP and other peroxidases. Second, the characterization of the differences in the heme of WT KatG and KatG(S315T) is pursued to determine structural criteria for INH activation.

EXPERIMENTAL METHODS

Protein Isolation and Sample Preparation. *Mtb* WT KatG and KatG(S315T) proteins were overexpressed and purified from *E. coli* using the previously reported protocol (*22*). Protein concentrations were determined using the Bradford assay with bovine serum albumin as the standard (*27*). WT KatG and KatG(S315T) samples at various pHs were obtained by dialysis against the desired buffer. The following buffers were used: 50 mM citric acid/sodium citrate, pH 5.0 and 5.3, 50 mM sodium phosphate, pH 7.5, 50 mM Tris/HCl, pH 7.8 and 8.0, and 50 mM glycine, pH 10.0.

Reduced WT KatG and KatG(S315T) samples were prepared anaerobically by addition of an aliquot of a fresh buffered stock sodium dithionite solution. The extent of reduction was evaluated by UV−visible spectroscopy. All UV−visible spectra were recorded on a scanning double beam spectrometer under microcomputer control at ambient temperature.

Fluoride complexes of the ferric KatG proteins were generated by titration with a 1 M buffered stock sodium fluoride solution until no further change was observed in the UV−visible and rR spectra. To ensure that an endpoint had been reached, spectra were also obtained after a final addition of solid NaF.

Resonance Raman Spectroscopy. Resonance Raman spectra were acquired using 406.7, 413.1, or 441.6 nm excitation from Kr^+ and HeCd lasers, respectively. UV−visible spectra were obtained before and after rR experiments to ensure that the samples were not irreversibly altered in the laser beam. Laser powers were between 0.2 and 20 mW at the sample, and spectral artifacts due to photoinduced chemistry were avoided by judicious control of the incident power. Samples ranging in concentration from 0.05 to 0.30 mM were spun at approximately 20 Hz in a 5-mm NMR tube at ambient temperature. Spectra were recorded using f1 collection optics, holographic notch filters, a 0.64-m spectrograph fitted with a 110 × 110 mm, 2400 groove/mm holographic grating, and a 1100-pixel CCD detection system. The spectrometer was calibrated with toluene, DMF, CCl_4, and CH_2Br_2 as frequency standards. Raman bands were fit using 50:50 Gaussian:Lorentzian band shapes that were allowed to vary in position, line width, and intensity to minimize χ^2.

ESR Spectroscopy. For ferric forms of the KatG proteins, ESR spectra were recorded at 15 K with a spectrometer operating at X-band microwave frequency (9.45 GHz) and equipped with a continuous-flow helium cryostat. Microwave power of 2 mW was used and shown to be nonsaturating for either the low spin (LS) or high spin (HS) components of the spectra. The relative proportion of HS and LS iron was estimated by simulating the spectra (Simfonia software, Bruker, version 1.2) and comparing the double integral area of HS and LS features. Integrals were corrected for *g* value differences according to the method of Aasa and Vängård (*28*).

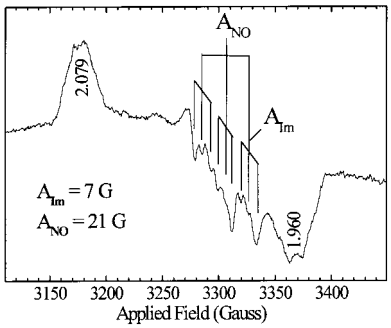

FIGURE 1: ESR spectrum of ferrous nitrosyl WT KatG. A_{Im} is the electron−nuclear hyperfine coupling constant for N_δ of the proximal histidine, and A_{NO} is that for the N nucleus of the NO ligand. The sample was 380 μM in WT KatG-NO and 80 mM in sodium phosphate, pH 7.5. Instrument parameters: temperature, 77 K; microwave power, 20 mW; field modulation amplitude, 5 G; spectrometer frequency, 9.240 GHz; field modulation frequency, 100 kHz; time constant, 1 s; and sweep width, 400 G.

The ferrous nitrosyl adduct was generated from ferric WT KatG by addition of 10 equiv of sodium dithionite (from a 0.15 M stock dithionite solution in 0.5 M sodium phosphate, pH 7.5) followed by exposure to 1 atm of NO. The ESR spectrum in Figure 1 was acquired at 9.240 GHz and 77 K. The ESR signals were referenced to solid pitch diluted in KCl.

RESULTS

Proximal Heme Ligation in KatG. The ESR spectrum of ferrous WT KatG-NO in Figure 1 is consistent with a six-coordinate (6-c) nitrosyl adduct where the proximal ligand is coordinated through a nitrogen atom (*29*). The g_z component is split into nine lines with hyperfine coupling constants of 21 and 7.0 G for the NO and proximal ligand nitrogens, respectively. The 7.0-G coupling is typical of a proximal His ligand (*30*). On the basis of multiple sequence alignments of KatG with class I catalase-peroxidases (*11*, *14*), we hypothesize that the proximal histidine corresponds to His270.

The proximal heme ligand is further identified as a histidine imidazolate by the vibrational band at 244 cm^{-1} in the Soret-excited rR spectra of HS ferrous WT KatG (Figure 2). Intense bands in this frequency range have been assigned to ν(Fe-His), the stretching vibration of the proximal Fe-histidine unit, for a number of heme peroxidases (*31*−*40*). The frequency obtained for WT KatG is compared with those of other peroxidases in Table 1. This ν(Fe-His) frequency is consistent with imidazolate character of the proximal histidine due to strong hydrogen bonding with an acidic residue (as in CCP and HRP) (∼245 cm^{-1}) (*33*−*37*, *39*). The band shifts toward slightly lower frequencies (∼241 cm^{-1}) as the pH is increased. This is consistent with a slight weakening of the Fe-imidazolate bond, and similar behavior is observed for HRP (*31*, *37*).

The rR spectrum of ferrous KatG(S315T) also confirms a histidine as its proximal ligand by the presence of an ν(Fe-His) stretch. At pH 8.0, the KatG(S315T) spectrum is similar to that of the WT protein as shown in Figure 2 and Table 1. A notable difference is a shoulder (∼228 cm^{-1}) observed

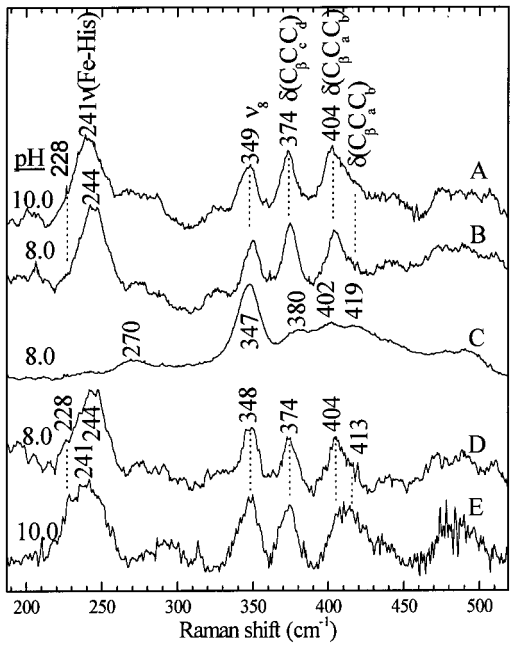

FIGURE 2: Low-frequency rR spectra of ferrous WT KatG and KatG(S315T). (A) WT KatG in 50 mM glycine buffer, pH 10.0, with 441.6-nm excitation; (B) WT KatG in 50 mM Tris/HCl, pH 8.0, with 441.6-nm excitation; (C) WT KatG in 50 mM Tris/HCl, pH 8.0, with 413.1-nm excitation; (D) KatG(S315T) in 50 mM Tris/HCl, pH 8.0, with 441.6-nm excitation; and (E) KatG(S315T) in 50 mM glycine buffer, pH 10.0, with 441.6-nm excitation.

Table 1: Iron-Histidine Stretching Frequencies for Ferrous Heme Proteins

	Fe(II)-histidine stretching frequencies (cm^{-1})[a]		
protein	imidazolate	imidazole	refs
WT KatG	244	228 sh (weak)	this work
KatG(S315T)	244	228 sh	this work
CCP	249	227 sh	*36*
CCP	246	233 sh	*34*, *35*, *39*
CIP	230	210	*38*
APX	234	207	*40*
HRP-C	243		*31*, *37*
HRP-A_2	252		*31*
TP-1	252		*33*
JRP-2	247		*33*
LPO	258		*34*
IP	254		*32*
Mb		220	*41*
R-state βHbA		224	*42*
T-state βHbA		220	*42*
R-state αHbA		218	*42*
T-state αHbA		203	*42*

[a] sh: shoulder.

on the 244 cm^{-1} band that can be seen more clearly at pH 10.0 (Figure 2E). This shoulder is tentatively assigned to a second ν(Fe-His) stretching frequency, consistent with weak hydrogen bonding to a neutral acceptor (e.g., Hb and Mb, ~220 cm^{-1}) (*31*, *41*−*45*). The 228-cm^{-1} shoulder observed for ferrous KatG(S315T) is present in the WT spectrum although it is relatively weak and not affected as dramatically by an increase in pH. One interpretation of two ν(Fe-His) stretching bands is that they represent at least two conformers with different hydrogen-bonding acceptors. For example, on the basis of sequence homology with CCP, the hydrogen-bonding acceptor for the 244-cm^{-1} band conformation is most likely the carboxylate of Asp381. A neutral hydrogen-bond acceptor, such as the leucine backbone carbonyl groups in Hb, would be the weaker acceptor responsible for the conformation reflected in the 228-cm^{-1} band. Alternatively, these ν(Fe-His) bands may arise from two tautomers, one where the hydrogen is on the anionic residue and the other where the hydrogen is bound to the proximal imidazole. Evidence for such tautomers has been reported for CCP (*46*), *Coprinus cinereus* peroxidase (CIP) (*38*), and ascorbate peroxidase (APX) (*40*). For comparison with the KatG data, their ν(Fe-His) frequencies and those of Hb are given in Table 1. With either interpretation, the S315T mutation in KatG affects the hydrogen-bonding environment of the proximal histidine in ferrous KatG at high pH.

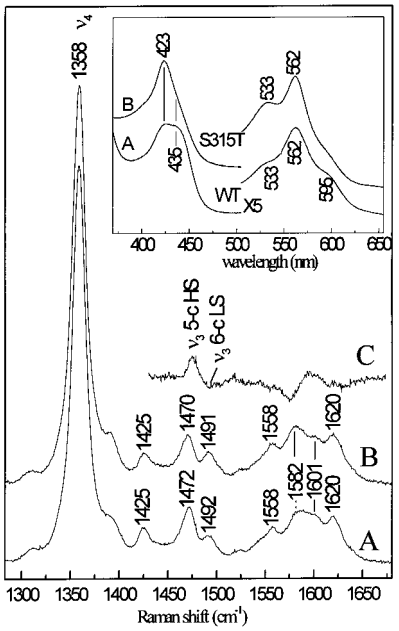

FIGURE 3: High-frequency rR spectra of ferrous WT KatG and KatG(S315T). (A) Ferrous WT KatG; (B) ferrous KatG(S315T); (C) difference spectrum, [WT KatG − KatG(S315T)] (spectrum A − spectrum B). Spectra were recorded with 413.1-nm excitation (8 mW). Samples were in 50 mM Tris/HCl, pH 8.0. Inset: UV−Visible spectra of reduced WT KatG (A) and KatG(S315T) (B) in 50 mM Tris/HCl, pH 8.0.

Coordination and Spin States of Ferrous WT KatG and KatG(S315T). Comparison of low-frequency rR spectra of ferrous WT KatG obtained with 441.6- and 413.1-nm excitation in Figure 2 reveals five-coordinate (5-c) HS and 6-c LS forms. Five-coordinate HS hemes are selectively resonance-enhanced with 441.6 nm excitation; the ν(Fe-His) stretching mode and the vinyl [$\delta(C_\beta C_a C_b)$] and propionate [$\delta(C_\beta C_c C_d)$] bending modes for 5-c HS WT KatG dominate the spectrum in Figure 2B. When 413.1-nm excitation is used (Figure 2C), a broad envelope between 340 and 430 cm^{-1} is consistent with overlapping bands from HS and LS species.

High-frequency Soret-excited rR spectra of the ferrous enzymes also show that both are mixtures of 5-c HS and 6-c LS species (Figure 3). The ν_3 vibration is sensitive to heme spin state and coordination number. The ferrous 5-c HS forms are identified by their ν_3 bands at 1472 cm^{-1} (WT) and 1470 cm^{-1} [KatG(S315T)]. The ferrous 6-c LS species have the ν_3 bands at 1492 and 1491 cm^{-1} for WT and mutant proteins, respectively. These frequencies are similar to those of ν_3 bands observed for ferrous 5-c HS and 6-c LS CCP

(*38*, *46*). A difference spectrum, obtained by subtraction of the rR spectra of KatG(S315T) from WT KatG with ν_4 bands of equal intensities, indicates that there is a difference in the HS:LS species ratio observed for the two proteins (Figure 3C) with more 5-c HS observed in ferrous WT KatG than in the mutant protein. However, since the cross-section of the ν_3 band of 5-c HS ferrous heme species is significantly larger than that of its corresponding 6-c LS ν_3 (*47*), it is not possible to interpret the ferrous KatG rR spectra in terms of actual concentrations of the two forms.

Visible spectra of ferrous WT and KatG(S315T) (inset, Figure 3) are consistent with the rR data. Broad B bands between 420 and 440 nm indicate the presence of at least two species, 5-c HS Fe(II) (λ_{max} 435 nm) and 6-c LS Fe(II) (λ_{max} 423 nm) (*47*). Q bands for 5-c HS and 6-c LS ferrous hemes are expected around 559/585 and 535/558 nm, respectively. Both sets of Q bands are observed in both the WT and KatG(S315T) spectra. While the band maxima in the two spectra appear similar, their intensities vary substantially between the WT and the mutant. The relative intensities of the 5-c HS and 6-c LS bands are consistent with a higher fraction of 5-c HS in ferrous WT than in KatG(S315T).

The larger 5-c HS:LS ratio observed for ferrous WT KatG relative to KatG(S315T) may be a result of an altered pK_a for a sixth ligand responsible for the spin-state transition in the two proteins. Precedence for a spin-state transition with a pK_a between 7.5 and 8.0 is found in ferrous CCP, which exists as a mixture of 5-c HS and 6-c LS species at pH > 7.6 (*47*−*49*). Alternatively, the mutation at the periphery of the heme in KatG(S315T) may result in a more flexible heme pocket that allows an easier approach of the distal histidine to the heme iron. Another possible explanation for the different HS:LS ratio may be variations in resonance enhancement due to electronically distinct species of the same spin state in the two proteins.

Coordination and Spin State of Ferric WT KatG and KatG(S315T). Ferric WT KatG and KatG(S315T) in 50 mM sodium phosphate, pH 7.5, were examined by rR spectroscopy with 413.1-nm excitation at room temperature (Figure 4). Assignments of the high-frequency rR bands for both proteins are given in Table 2. The ν_3 band, whose frequency is sensitive to spin state and coordination number, indicates that ferric WT KatG exists in at least two forms at pH 7.5. In ferric heme spectra, the ν_3 envelope is observed between 1475 and 1485 cm^{-1} for 6-c HS species, between 1490 and 1500 cm^{-1} for 5-c HS species, and between 1500 and 1510 cm^{-1} for 6-c LS forms (*53*, *54*). WT KatG exhibits a broad envelope in this region (Figure 4A). When curve fit to two peaks, the calculated Raman shifts are 1490 and 1502 cm^{-1}. These frequencies indicate a mixture of 5-c HS and 6-c LS species. Even though the ν_3 envelope obtained with 413.1-nm excitation can be fit to two bands, there is intensity between 1480 and 1485 cm^{-1} in both the 413.1- and 406.7-nm excited spectra (Figure 5B, inset). Therefore, the presence of 6-c HS ferric heme in WT KatG cannot be discounted and would not be surprising, since other heme peroxidases are known to be HS 6-c aqua complexes in their resting states (*37*, *50*, *51*).

When the ν_3 region of KatG(S315T) is fit to two bands, their frequencies are the same as those obtained from fits for WT KatG. Thus, the porphyrin core size appears unaffected by the mutation. The difference spectrum (WT-S315T) (Figure 4C) and the simulated spectra shown in Figure 4, panels A and B suggest that the difference features observed for ν_3, ν_2, and ν_{10} are a result of varying intensities of these bands in the spectra of the two proteins. Hence, either the ratio of HS:6-c LS species is higher in WT KatG than in KatG(S315T), or the electronic environments of the HS and 6-c LS species in the two proteins are different, resulting in altered resonance enhancements.

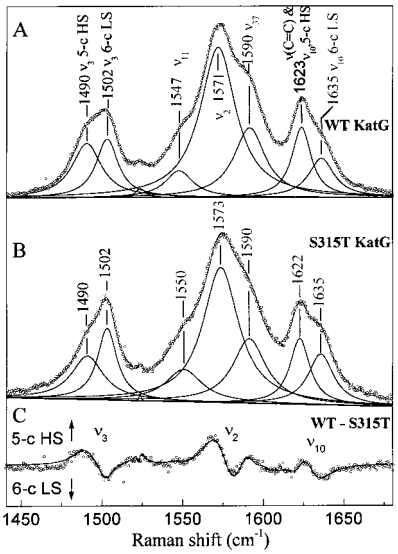

FIGURE 4: Resonance Raman spectra of ferric WT (A) and KatG(S315T) (B) in 50 mM phosphate, pH 7.5, using 413.1-nm excitation. The difference spectrum, (A − B) [WT KatG − KatG(S315T)], is shown in (C). Original data are shown as points; simulated spectra are shown as solid lines. Spectra were acquired with 5 mW laser power at the sample.

Since the amount of 6-c LS ferric CCP is known to increase with the age of the protein (*36*), high-frequency rR spectra of fresh (never frozen) WT KatG and KatG(S315T) were compared to those obtained from protein that had been stored frozen (−20 °C) for several months. Speciation differences were not detected. Since speciation of aged CCP is also phosphate-dependent (*36*), the high-frequency rR spectra of WT KatG obtained in 50 mM phosphate, pH 7.5, and 50 mM Tris/HCl, pH 8.0, were examined (data not shown). Their ratios of 1490 to 1502 cm^{-1} intensity were indistinguishable. Similar results were obtained for KatG(S315T).

Formation of a 6-c LS complex has been correlated with irradiation power and duration for ferric CIP (*38*). However, the HS/LS intensity ratio of ν_3-bands for KatG(S315T) is independent of laser power between 0.2 and 8 mW at the sample. Increased irradiation times (with 15 mW at sample) also did not cause a detectable increase in the KatG(S315T) 6-c LS population. Thus, formation of 6-c LS heme due to laser photolysis or protein instability during irradiation is unlikely. Resonance enhancement of ν_3 scattering by 5-c HS KatG(S315T) is greater with 406.7-nm excitation than at 413.1-nm (Figure 5D inset). With 406.7-nm excitation at neutral pH, it is clear that both 5-c HS and 6-c LS species are present in KatG(S315T).

The position of the ν_4 band is known for its sensitivity to oxidation state and porphyrin π^* electron density. For WT KatG and KatG(S315T), the ν_4 band is observed at 1373

Table 2: Comparison of Tentative RR Band Assignments of Ferric WT KatG and KatG(S315T) with Those of Other Ferric Peroxidases[a]

	WT KatG[b]		KatG(S315T)[b]		CIP	CCP	APX		MnP		SBP	HRP−C[c]	
vibration	5-c HS	6-c LS	5-c HS	6-c LS	5-c HS	5-c HS	5-c HS	6-c LS	6-c HS	5-c HS	5-c HS	6-c HS#	5-c HS#
$\delta(=CH_2)$	1426		1430		1428	1430	nr		1431		1428	1427	
ν_3	1490	1502	1490	1502	1492	1494	1493	1504	1482	1492	1492	1491*	1499*
ν_{11}	1547		1550			1551	1550	1566	1549		1550	1547	1553
ν_2	1571		1573		1566	1570	1571	1577	1564		nr	1566	1572
ν_{10}	1635		1635		1631	1629	1629	1638	1612	1628	1633	1620*	1636*
ν_{37}	1590		1590		1584	1588	1583	1602	nr		nr	1579	1584
ν(C=C)	1623		1622		1622	1620	1623		1623		nr	1624	
							1629					1630	
ref	this work		this work		*38*	*36*	*40*		*50*, *51*		*52*	*37*	

[a] nr, not reported; HS, high-spin; LS, low-spin. [b] Data for proteins at pH 7.5 are reported. Because of extensive overlap of bands, it is not possible to assign core size marker band frequencies between 1525 and 1640 cm^{-1} for the various HS and LS species. [c] 6-c HS# and 5-c HS# are used to distinguish these from "normal" hemes. It has been shown that the frequencies for the ν_3 and ν_{10} core size marker bands for HRP-C are approximately 10 cm^{-1} higher than those normally observed for 6-c HS and 5-c HS hemes in models and other proteins. They have been marked with an asterisk indicating that they are atypical frequencies. It has been suggested that this is due to a different degree of distortion from planarity or a more contracted core in the HS heme of HRP-C relative to other heme proteins.

cm^{-1} (Figure 5, panels B and D), a frequency typical of Fe(III) hemes. This rules out the possibility that one or more of the ν_3 bands is due to ferrous heme produced via laser-induced photoreduction. If ferrous KatG were present, there would be a ν_4 band near 1358 cm^{-1} (see Figure 3).

To probe potentially different responses of the hemes and their distal pockets to changes in pH, the high-frequency rR signatures of WT KatG and KatG(S315T) were recorded between pH 5.0 and 10.0 as shown in Figure 5, panels B and D. The ν_3 envelope for WT KatG indicates that there is a small shift of intensity from 5-c HS (or 6-c HS) heme to 6-c LS heme as the pH is raised. Unlike CCP, which contains predominantly 5-c HS heme at pH ≤ 7 and exists as a 6-c LS bis-histidine complex in alkaline solution (*34*, *55*−*57*), complete conversion to a single coordination and spin state does not occur in ferric KatG in the pH range examined. KatG(S315T) behaves more like CCP with the LS heme (as judged by ν_3 band, Figure 5D) becoming the predominant species as the pH is raised. To differing degrees, the pockets of both proteins respond to pH in a way consistent with conformational flexibility in the distal heme pocket.

Changes in the low-frequency spectra of ferric WT KatG and KatG(S315T) with varying pH (Figure 5, panels A and C) are also consistent with multiple spin states. By analogy with CCP (*35*, *39*), the following assignments were made: 404 cm^{-1}, $\delta(C_\beta C_a C_b)$ bending mode of the heme vinyl substituents of 5-c HS and 6-c LS hemes; 422 cm^{-1} [421 cm^{-1}, KatG(S315T)], second $\delta(C_\beta C_a C_b)$ mode observed for 6-c LS hemes; 378 cm^{-1}, $\delta(C_\beta C_c C_d)$ propionate bending mode; 349 cm^{-1}, ν_8; and 337 cm^{-1}, γ_6 out-of-plane porphine mode. For WT KatG at pH 5.0, the 422-cm^{-1} band is a small shoulder on the 404-cm^{-1} band. As the pH is raised, the 404-cm^{-1} band broadens, the vinyl mode due to the 6-c LS species grows in intensity, and the intensity of γ_6, which appears as a shoulder on ν_8, decreases relative to ν_8. The γ_6 band is not observed for 6-c LS heme. Its intensity increases with equilibrium out-of-plane distortions of the porphyrin. Its relative intensity is higher for 5-c HS than for 6-c HS heme, probably due to larger doming of the porphyrin in the 5-c form (*34*, *35*, *55*, *58*). Hence, all the spectral changes observed are consistent with conversion of 5-c HS and/or 6-c HS heme to 6-c LS heme as the pH is raised. Similar behavior is observed for ferric KatG(S315T) (Figure 5C), except that the HS γ_6 band at 337 cm^{-1} is barely detectable at pH ≥ 7.5. Like the high-frequency data, this suggests that less HS heme is present in the mutant than in WT KatG at physiological pH.

Multiple species are also evident in the UV−visible absorbance spectra of WT KatG and KatG(S315T) at pH 5.1 and 7.8 in Figure 6. The porphyrin to iron charge-transfer band [a'_{2u} (π) → $e_g(d_\pi)$] CT1, is only observed for HS heme proteins. It occurs between 600 and 637 nm for 6-c HS heme proteins with a proximal histidine ligand and between 640 and 652 nm for 5-c HS heme proteins (*59*, *60*). For WT KatG at pH 7.8 (Figure 6A), CT1 is broad and occurs between 631 and 648 nm, suggesting a mixture of 5-c HS and 6-c HS species with a water molecule as the sixth ligand. The difference spectrum in Figure 6B [(pH 7.8)−(0.9)(pH 5.1)] was obtained using the CT1 band as a subtraction standard for removal of the HS contributions to the absorbance spectrum. A weighting factor for the pH 5.1 spectrum of 0.9 was required for complete subtraction of the CT1 features. Thus, the resulting difference spectrum (Figure 6B; 410-nm B band, 536/566-nm Q bands) is consistent with conversion of 10% of the HS heme present at pH 5.1 to a 6-c LS species (Table 3) at pH 7.8. Using a typical molar absorptivity for 6-c LS ferric hemes (100 000 M^{-1} cm^{-1}) (*45*), the absorbance due to LS heme in the difference spectrum accounts for the 10% loss of HS heme at pH 5.1. This HS → 6-c LS conversion is also detected in the visible spectra of KatG(S315T) (Figure 6, panels C and D). The difference spectrum [(pH 7.8)−(0.7)(pH 5.1)] has a B band λ_{max} = 412 nm and Q bands at 539 and 569 nm. On the basis of the 0.7 weighting factor necessary to remove the HS contribution at pH 7.8, 30% of the HS heme is converted to 6-c LS heme upon raising the pH from 5.1 to 7.8 for KatG(S315T). The room temperature UV−visible spectra are consistent with the rR data in that they show a larger fraction of the HS heme present at pH 5.1 is converted to the 6-c LS form at pH 7.8 in KatG(S315T) than in the WT enzyme (30 vs 10%, respectively). This analysis relies upon the reasonable assumption that their HS hemes have similar molar absorptivities.

To determine whether the sixth ligand of the 6-c LS complex is a weak-field ligand like water or hydroxide or a strong-field ligand such as a distal histidine, fluoride binding to the ferric KatGs was examined by rR spectroscopy. Fluoride complexes of heme proteins are 6-c and HS (*34*,

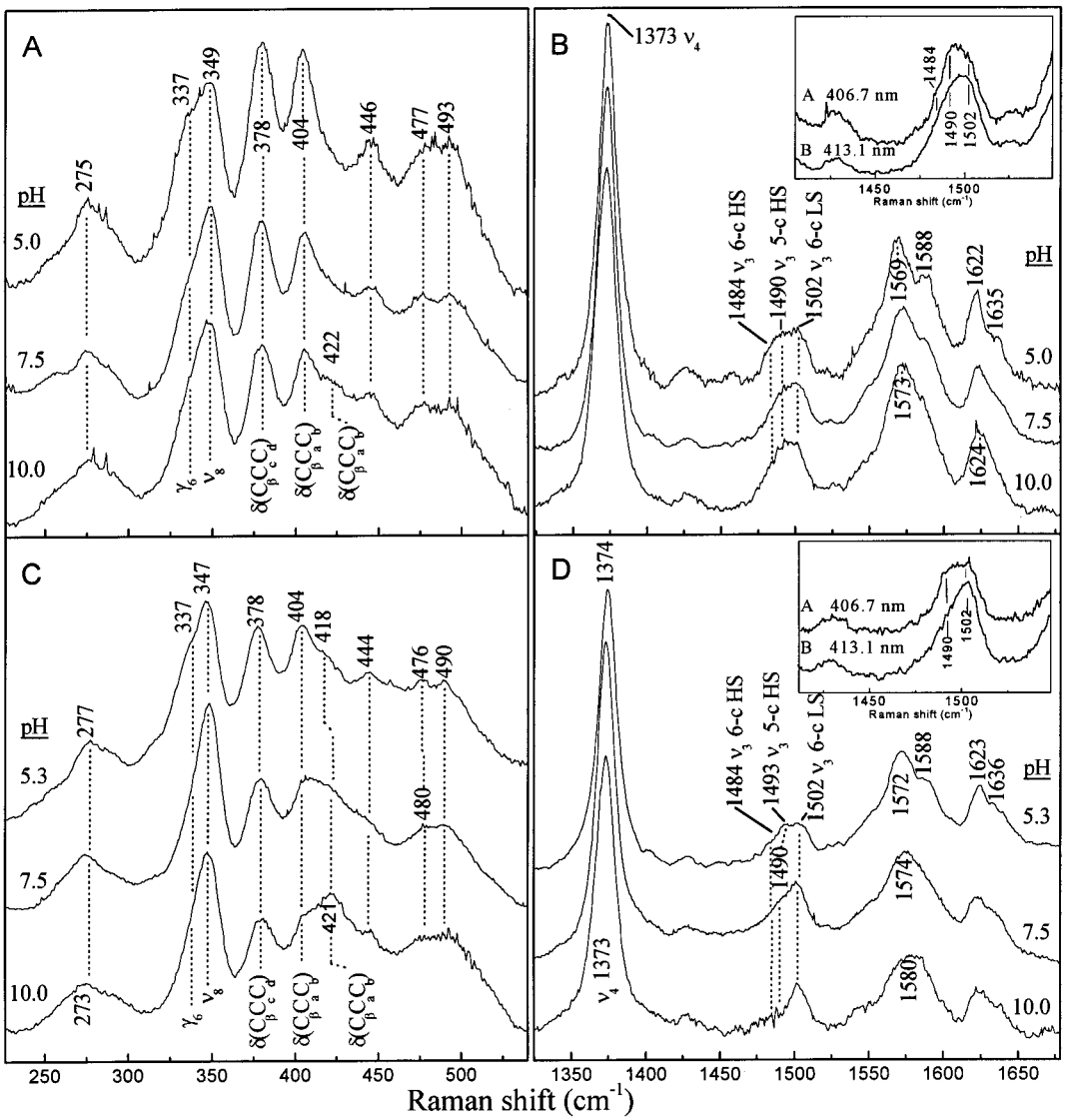

FIGURE 5: pH dependence of the rR spectra of ferric WT KatG and KatG(S315T). (Panels A and B) WT KatG; (panels C and D) KatG-(S315T). Spectra were acquired with 413.1-nm excitation and 5 mW laser power at the sample. Panel B, inset: comparison of ν_3 region of WT KatG in 50 mM phosphate, pH 7.5, with (A) 406.7-nm excitation and (B) 413.1-nm excitation. Panel D inset: comparison of ν_3 region for KatG(S315T) in 50 mM phosphate, pH 7.5, with (A) 406.7-nm and (B) 413.1-nm excitation.

69, *70*). The ν_3 envelope was monitored to determine whether all of the enzyme could be converted to the 6-c HS fluoride complex. At saturating NaF concentrations, both WT KatG and KatG(S315T) exhibit two species as indicated by two ν_3 bands. At pH 8.0 (Figure 7C), the 5-c HS WT KatG (ν_3, 1490 cm^{-1}) is converted into 6-c HS KatG-F with a ν_3 band at 1480 cm^{-1}, which is consistent with ν_3 frequencies observed for 6-c HS fluoride complexes of CCP, HRP, and CIP (*70*). However, the 6-c LS (ν_3, 1502 cm^{-1}) complex remains intact and presumably inaccessible for binding F^-. At pH 5.3, a considerably larger fraction of the ν_3 intensity is observed at 1480 cm^{-1}, suggesting that 6-c HS WT KatG-F is the predominant species (Figure 7A). The apparent increase in fluoride affinity may be partially due to a larger percentage of HS heme present for fluoride to complex at pH 5.3. Also, peroxidases are known to have a higher affinity for fluoride at acidic pH relative to alkaline conditions (*71*, *72*) due to stabilization of the ligand by hydrogen bonding. However, the 1502-cm^{-1} ν_3 band of 6-c LS WT KatG is still detected, so not all of the protein is converted to the fluoride adduct. Similar behavior was observed for KatG(S315T) reactivity with fluoride (Figure 7, panels B and D). At pH 8.0, HS KatG(S315T)-F (ν_3, 1479 cm^{-1}) and the 6-c LS (ν_3, 1502 cm^{-1}) species are observed. Even at [NaF] > 300 mM (> 6000-fold excess), the 6-c LS ν_3 (1502 cm^{-1}) persists. At pH 5.3, most of the ν_3 intensity is attributable to the HS fluoride complex. However, even with a large excess of sodium fluoride, some 6-c LS KatG(S315T) is still detected. These data suggest that the sixth ligand of the 6-c LS KatGs is not totally displaced by fluoride ion even under conditions where peroxidases such as CCP and HRP are completely converted to the fluoride adduct. Destablization of the 6-c LS species at low pH is consistent with protonation of a neutral nitrogen donor. These lines of evidence are consistent with a distal histidine as the sixth ligand of the LS adduct.

Interestingly, under conditions where CIP (*63*) and APX (*40*) readily form 6-c imidazole complexes, addition of imidazole to WT KatG did not yield a bis-imidazole complex. Very slight changes are observed in the Q-bands, and the broad CT1 band remains a distinctive feature in the

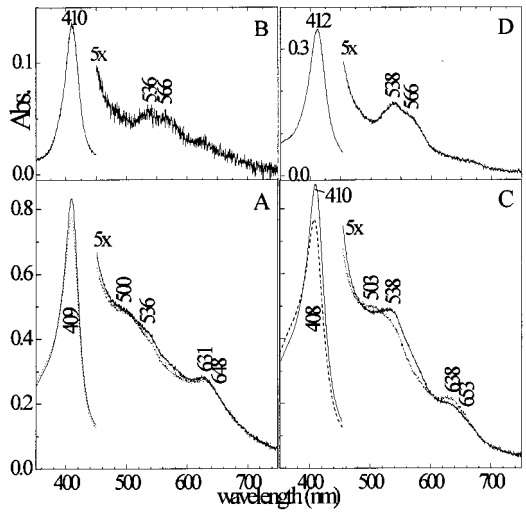

FIGURE 6: UV−Visible spectra of ferric WT KatG and KatG(S315T) at two different pHs. (A) WT KatG in 100 mM Tris/HCl, pH 7.8, solid line; WT KatG in 100 mM citrate, pH 5.1, dashed line. The protein was 7.4 μM at both pH 7.8 and pH 5.1. (B) Difference spectrum of [(WT KatG pH 7.8) − (0.9)(WT KatG pH 5.1)]. (C) KatG(S315T) in 100 mM Tris/HCl, pH 7.8, solid line; KatG(S315T) in 100 mM citrate, pH 5.1, dashed line. The absorbance axis for the Soret region is the same as in panel A. The KatG(S315T) concentration is 7.8 μM at both pHs. (D) Difference spectrum of [(KatG(S315T), pH 7.8) − (0.7)(KatG(S315T), pH 5.1)].

spectrum, even after adding a large excess of solid imidazole (data not shown). In contrast, a ferric KatG(S315T)−imidazole complex forms upon addition of excess imidazole at pH 10.0 as evidenced by its typical LS visible spectrum (B band at 411 nm, Q bands at 565 and 535 nm, data not shown). Comparison of the visible spectra of this exogenous imidazole adduct, known 6-c LS heme imidazole and hydroxide adducts, and 6-c LS KatG(S315T) in Table 3 is further evidence and strongly suggests that the sixth ligand in 6-c LS KatG(S315T) is the distal histidine (His108).

The LS and HS components of ferric WT KatG and KatG(S315T) are clearly seen in the 15-K ESR spectra in Figure 8. While UV−visible spectra (Figure 6, panels A and B) and NMR studies of WT KatG indicate a predominantly HS configuration at room temperature (S. Todorovic and F. Rusnak, unpublished results), quantitation of the 15-K ESR spectra reveal that LS heme states are favored at low temperature (79% LS WT KatG, 53% LS KatG(S315T), T = 15 K). Similar formation of 6-c LS species has been observed for CCP (*46*, *73*, *74*), APX (*40*, *75*), and HRP (*76*) upon freezing. Formation of 6-c LS CCP at cryogenic temperatures is prevented by addition of glycerol (*74*). However, addition of glycerol does not alter the low-temperature ESR spectrum of WT KatG.

The predominant LS component of WT KatG is characterized by a $g_z = 3.24$, $g_y = 2.05$, and $g_x = 1.28$. The position on a crystal field correlation diagram of LS ferric hemoproteins, a plot of tetragonality versus rhombicity, indicates a specific structural type (*77*). These parameters for WT KatG fall outside of the traditional bis-imidazole domain. There are several possible explanations for the large "g_{max}" value for LS WT KatG. One is that the LS adduct is a bis-imidazole complex with the imidazole planes nearly mutually orthogonal (*78*). Another explanation is that the sixth ligand in the LS WT KatG adduct is not a histidine. Large g_{max} values have been reported for complexes with histidine-methionine ligation (*79*−*81*) or with histidine-primary amino group ligation (*82*). However, on the basis of homology modeling with CCP, we favor assignment of His108 as the sixth ligand.

Table 3: Electronic Spectral Data of Some Low-spin Fe(III) Complexes[a]

protein	pH	B band	Q bands β	Q bands α	refs
WT KatG	7.8	410	536	566	this work
KatG(S315T)	7.8	412	539	569	this work
bis-imidazole complexes					
KatG(S315T)-Im	10.0	411	535	565	this work
cytochrome b_5	5.5	413	532	560	*61*
CCP(MI)	9.5	415	534	564	*35*
CCP, −190 °C	8.4	416	535	560	*62*
CIP-Im	10.0	412	534	560	*63*
APX-Im	10.0	411	535	559	*40*
$[Fe(PPIXDME)(ImH)_2]^+$		412	536.5	563	*64*
Fe(PPIXDME)(ImH)(Im)		414	540	565	*64*
heme 6-c imidazole, hydroxide complexes					
hemoglobin-OH	>9	410	540	575	*65*
myoglobin-OH	>9	411	541	582	*66*
HRP−OH	>11	416	545	572	*67*
CIP−OH	12.1	412	543	575	*68*
$[Fe(PPIXDME)(Im)(OH)]^-$		412	549.5	577.5	*64*

[a] Abbreviations: PPIX·DME, dianion of protoporphyrin IX dimethyl ester; ImH, imidazole; Im, imidazolate; CCP(MI), CCP with extra N-terminal methionine and isoleucine residues; 6-c, six-coordinate.

The LS component of KatG(S315T) has $g_z = 2.48$, $g_y = 2.28$, and $g_x = 1.88$. These g values yield tetragonality (Δ/λ) and rhombicity (V/Δ) parameters of $\Delta/\lambda = 4.50$ and $V/\Delta = 0.93$, which place KatG(S315T) in domain H of the crystal field correlation diagram for LS ferric heme proteins (bis-imidazole with one or both histidines deprotonated) (*77*).

Examination of the ESR spectra after addition of sodium fluoride to ferric WT KatG and KatG(S315T) (Figure 8) at pH 7.8 indicates that only the HS species are converted to the 6-c HS fluoride complex. Both rR and ESR data indicate that the 6-c LS species remain intact, suggesting that fluoride is unable to compete with the sixth ligand for binding to the heme iron. Hence, the rR, visible, and ESR spectral data are all consistent with an endogenous strong-field sixth ligand, probably His108, in ferric 6-c LS WT KatG and KatG(S315T).

DISCUSSION

Data presented here indicate that the proximal ligation of the heme in WT KatG is a histidine with imidazolate character similar to peroxidases such as HRP and CCP. Regardless of oxidation state, WT KatG exists primarily in a HS state in the neutral pH range where INH turnover is optimal. In the ferric form, ESR signatures of three HS species (*25*) and at least one 6-c LS species are observed for WT KatG. Two rhombic ESR features consistent with two 5-c HS species and an axial ESR spectrum of a 6-c HS species are present. This is consistent with the visible and rR data that indicate both 6-c and 5-c HS species at ambient temperature. On the basis of its CT1 band, the ferric 6-c HS form of WT KatG probably has water as its sixth ligand (*60*). The LS species observed in ESR spectra reported here were missed in earlier reports because they are readily saturated under the previously used temperature and power conditions.

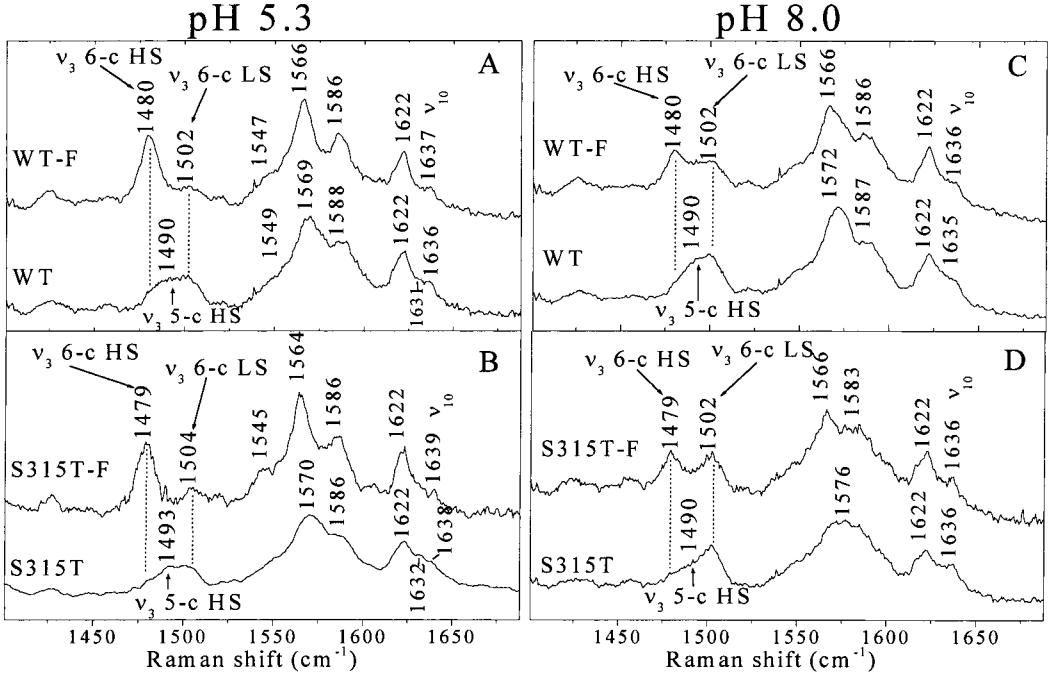

FIGURE 7: Resonance Raman spectra of ferric WT KatG and KatG(S315T) titrated with sodium fluoride. (A) WT KatG in 50 mM citrate, pH 5.3; top: 120 mM NaF; bottom: no NaF. (B) KatG(S315T) in 50 mM, pH 5.3; top: 120 mM NaF; bottom: no NaF. (C) WT KatG in 25 mM Tris/HCl, pH 8.0; top: 250 mM NaF; bottom: no NaF. (D) KatG(S315T) in 25 mM Tris/HCl, pH 8.0; top: 300 mM NaF; bottom: no NaF. Spectra were obtained with 413.1-nm excitation; laser power at the sample was 12 mW.

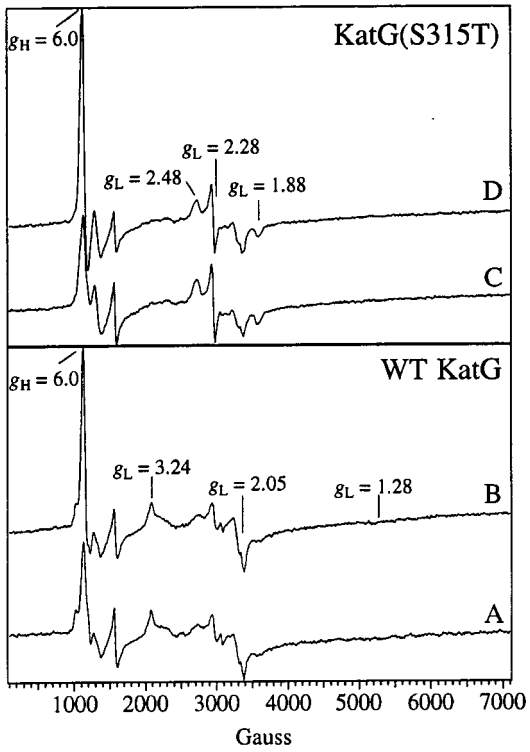

FIGURE 8: ESR spectra of ferric KatG proteins in the absence and presence of NaF. The H and L subscripts indicate HS and LS contributions to the spectrum, respectively. (A) WT KatG. (B) WT KatG plus NaF. (C) KatG(S315T). (D) KatG(S315T) plus NaF. Parameters: pH 7.8; temperature, 15 K; microwave power, 2 mW; field modulation amplitude, 10.4 G; spectrometer frequency, 9.454 GHz; field modulation frequency, 100 kHz; time constant, 164 ms; and sweep width, 7000 G.

The large "g_{max}" LS ESR spectrum for 6-c LS WT KatG leaves some question as to the identity of the endogenous distal ligand. Although the amount of 6-c LS WT KatG at room temperature is small, its presence suggests an axial ligand that may play a role in defining accessibility of substrates and/or oxidants (e.g., superoxide) to the heme iron. Indeed, the fact that freezing the sample produces a majority of WT KatG in a 6-c LS state indicates that this ligand is near the heme iron and accessible enough that its coordination to the iron can be driven by reducing the temperature.

Comparison of the ESR signatures of the recombinant ferric 6-c LS WT KatG and KatG(S315T) reported here reveals a difference in the 6-c LS species. The ESR spectrum of the 6-c LS species of KatG(S315T) is consistent with a bis-imidazole complex. Precedence for such a species is found in CCP (*48*, *49*). Spectroscopic characterization of CCP and CCP(H52L) have shown that the 6-c LS complex formed in alkaline solution is a bis-imidazole species with the distal His52 coordinating to the heme iron (*46*). By sequence homology with CCP, the most likely candidate in KatG(S315T) is the distal imidazole of His108 (*11*, *14*). If His108 is also the distal ligand in 6-c LS WT KatG, the ESR spectrum indicates that its geometry in the distal pocket (nearly perpendicular to the proximal imidazole plane) is different from that in KatG(S315T). Since INH has been shown by NMR to bind near the heme periphery (*25*, *26*), differences in identity or environment of the axial heme ligands in the LS WT and KatG(S315T) may be determining factors in INH resistance.

ESR integrations indicate larger amounts of LS species in WT KatG than in KatG(S315T) at 15 K. This is in contrast to the room temperature (pH 7.8) UV−visible absorbance and rR data that indicate more 6-c LS in KatG(S315T) than in WT KatG. However, freezing of heme protein solutions has been known to change spin state and coordination number (*40*, *73*−*76*). It is possible that the altered distal heme pocket responsible for the differing 6-c LS WT and KatG-(S315T) ESR signatures is differentially affected by forces

associated with freezing.

In contrast to the low-temperature ESR results, UV−visible and rR spectra carried out at near-physiological (ambient) temperature indicate a higher fraction of 6-c LS KatG(S315T), wherein the heme iron is less accessible for binding exogenous ligands, e.g., superoxide (which binds to ferric KatG) or O_2 (which binds to ferrous KatG). Since it has been proposed that oxyKatG is an intermediate in INH oxidation (*24*, *83*), the increase in the fraction of 6-c LS heme reported here for KatG(S315T) could be critical, as it may decrease access of O_2 or superoxide to the heme iron. Because the population of 6-c LS hemes is greater in both ferrous and ferric forms of KatG(S315T) relative to the WT, the yield of oxyKatG(S315T) could be diminished whether it is formed by reaction of Fe(II) with O_2 or Fe(III) with superoxide. This may be one factor in determining INH resistance afforded by the S315T mutation. However, it is difficult to attribute all the 8−11-fold difference in INH turnover rates of these enzymes (*22*, *24*) to the 2−3-fold increase in 6-c LS KatG(S315T) as compared to WT KatG. A second contributing factor to the altered reactivity of the mutant toward INH may be mutation-induced electronic and/or steric differences in the distal heme pocket. Although NMR and competitive inhibition studies indicate that INH binds approximately the same distance from the heme iron and with the same affinity for WT KatG and KatG(S315T) (*25*, *26*), these results do not eliminate the possibility that INH is bound to KatG(S315T) in a nonoptimal orientation. Taken together, these results provide evidence for an altered distal heme environment in KatG(S315T) versus WT that may account for its diminished reactivity toward either oxidant or INH itself.

REFERENCES

1. World Health Organization (1998) *World Health Report.*
2. Moore, M, Onorato, I. M., McCray, E., and Castro, K. G. (1997) *JAMA 278*, 833−837.
3. World Health Organization (1997) *Anti-Tuberculosis Drug Resistance in the World*.
4. Mitchison, D. A. (1985) *Tubercle 66*, 219−225.
5. Stratton, M. A., and Reed, M. T. (1986) *Clin. Pharm. 5*, 977−987.
6. Riley, L. W. (1996) In *Tuberculosis* (Rom, W. N., Gary, S., Eds.) pp. 763−771, Little Brown & Company, Boston.
7. Banerjee, A., Dubnau, E., Quemard, A., Balasubramanian, V., Um, K. S., Wilson, T., Collins, D., deLisle, G., and Jacobs, W. R., Jr. (1994) *Science 263*, 227−230.
8. Quemard, A., Sacchettini, J. C., Dessen, A., Vilcheze, C., Bittman, R., Jacobs, W. R., Jr., and Blanchard, J. S. (1995) *Biochemistry 34*, 8235−8241.
9. Mdluli, K., Slayden, R. A., Zhu, Y., Ramaswamy, S., Pan, X., Mead, D., Crane, D. D., Musser, J. M., and Barry, C. E., III. (1998) *Science 280*, 1607−1610.
10. Cockerill, F. R., III, Uhl, J. R., Temesgen, Z., Zhang, Y., Stockman, L., Roberts, G. D., Williams, D. L., and Kline, B. C. (1995) *J. Infect. Dis. 171*, 240−245.
11. Heym, B., Alzari, P. M., Honore, N., and Cole, S. T. (1995) *Mol. Microbiol. 15*, 235−245.
12. Musser, J. M., Kapur, V., Williams, D. L., Kreiswirth, B. N., van Soolingen, D., and van Embden, J. D. A. (1996) *J. Infect. Dis. 173*, 196−202.
13. Ramaswamy, S., and Musser, J. M. (1998) *Tubercle and Lung Disease 79*, 3−29.
14. Heym, B., Zhang, Y., Poulet, S., Young, D., and Cole, S. T. (1993) *J. Bacteriol. 175*, 4255−4259.
15. Haas, W. H., Schilke, K., Brand, J., Amthor, B., Weyer, K., Fourie, P. B., Betzel, G., Sticht-Groh, V., and Bremer, H. J. (1997) *Antimicrob. Agents Chemother. 41*, 1601−1603.
16. Marttila, H. J., Soini, H., Eerola, E., Vyshnevakaya, E., Vyshnevskiy, B. I., Otten, T. F., Vasilyef, A. V., and Viljanen, M. K. (1998) *Antimicrob. Agents Chemother. 42*, 2443−2445.
17. Zhang, Y., Heym, B., Allen, B., Young, D., and Cole, S. (1992) *Nature 358*, 591−593.
18. Zhang, Y., Garbe, T., and Young, D. (1993) *Mol. Microbiol. 8*, 521−524.
19. Marcinkeviciene, J. A., Magliozzo, R. S., and Blanchard, J. S. (1995) *J. Biol. Chem. 270*, 22290−22295.
20. Johnson, K., Froland, W. A., and Schultz, P. G. (1997) *J. Biol. Chem. 272*, 2834−2840.
21. Nagy, J. M., Cass, A. E. G., and Brown, K. A. (1997) *J. Biol. Chem. 272*, 31265−31271.
22. Wengenack, N. L., Uhl, J. R., St. Amand, A. L., Tomlinson, A. J., Benson, L. M., Naylor, S., Kline, B. C., Cockerill, F. R., III, and Rusnak, F. (1997) *J. Infect. Dis. 176*, 722−777.
23. Saint-Joanis, B., Souchon, H., Wilming, M., Johnsson, K., Alzari, P. M., and Cole, S. T. (1999) *Biochem. J. 338*, 753−760.
24. Wengenack, N. L., Hoard, H. M., and Rusnak, F. (1999) *J. Am. Chem. Soc. 121*, 9748−9749.
25. Wengenack, N. L., Todorovic, S., Yu, L., and Rusnak, F. (1998) *Biochemistry 37*, 15825−15834.
26. Todorovic, S., Juranic, N., Mucura, S., and Rusnak, F. (1999) *J. Am. Chem. Soc. 121*, 10962−10966.
27. Bradford, M. M. (1976) *Anal. Biochem. 72*, 248−254.
28. Aasa, R., and Vängård, T. (1975) *J. Magn. Reson. 18*, 308−315.
29. Palmer G. (1983) in *Iron Porphyrins, Part II* (Lever, ABP, Gray HB, Eds.) pp 43−88, Addison-Wesley Publishing Company, Reading, Massachusetts.
30. Henry, Y., and Mazza, G. (1974) *Biochim. Biophys. Acta 371*, 14−19.
31. Teraoka, J., and Kitagawa, T. (1981) *J. Biol. Chem. 256*, 3969−3977.
32. Kimura, S., Yamazaki, I., and Kitagawa T. (1981) *Biochemistry 20*, 4632−4638.
33. Teroka, J., Job, D., Morita, Y., and Kitagawa, T. (1983) *Biochim. Biophys. Acta 747*, 10−15.
34. Hashimoto, S., Teraoka, J., Inubushi, T., Yonetoni, T., and Kitagawa, T. (1986) *J. Biol. Chem. 261*, 11110−11118.
35. Smulevich, G., Mauro, J. M., Fishel, L. F., English, A. M., Kraut, J., and Spiro, T. G. (1988) *Biochemistry 27*, 5477−5485.
36. Dasgupta, S., Rousseau, D. L., Anni, H., and Yonetani, T. (1989) *J. Biol. Chem. 264*, 654−662.
37. Smulevich, G., Paoli, M., Burke, J. F., Sanders, S. A., Thorneley, R. N. F., and Smith, A. T. (1994) *Biochemistry 33*, 7398−7407.
38. Smulevich, G., Feis, A., Focardi, C., Tams, J., and Welinder, K. G. (1994) *Biochemistry 33*, 15425−15432.
39. Smulevich, G., Hu, S., Rodgers, K. R., Goodin, D. B., Smith, K. M., and Spiro, T. G. (1996) *Biospectroscopy 2*, 365−376.
40. Nissum, M., Neri, F., Mandelman, D., Poulos, T. L., and Smulevich, G. (1998) *Biochemistry 37*, 8080−8087.
41. Kitagawa, T., Nagai, K., and Tsubaki, M. (1979) *FEBS Lett. 104*, 376−378.
42. Nagai, K., and Kitagawa, T. (1980) *Proc. Natl. Acad. Sci. U.S.A. 77*, 2033−2037.
43. Nagai, K., Kitagawa, T., and Morimoto, H. (1980) *J. Mol. Biol. 136*, 271−289.
44. Benko, B., and Yu, N.-T. (1983) *Proc. Natl. Acad. Sci. U.S.A. 80*, 7042−7047.
45. Teraoka, J., and Kitagawa, T. (1980) *Biochem. Biophys. Res. Commun. 93*, 694−700.
46. Smulevich, G., Miller, M. A., Kraut, J., and Spiro, T. G. (1991) *Biochemistry 30*, 9546−9558.
47. Wang, J., Boldt, N. J., and Ondrias, M. R. (1992) *Biochemistry 31*, 867−878.
48. Shelnutt, J. A., Satterlee, J. D., and Erman, J. E. (1983) *J. Biol. Chem. 25*, 2168−2173.

49. Conroy, C. W., Tyma, P., Daum, P. H., and Erman, J. E. (1978) *Biochim. Biophys. Acta 537*, 62−69.
50. Mino, Y., Wariishi, H., Blackburn, N. J., Loehr, T. M., and Gold, M. H. (1988) *J. Biol. Chem. 263*, 7029−7036.
51. Kishi, K., Kusters-van Someren, M., Mayfield, M. B., Sun, J., Loehr, T. M., and Gold, M. H. (1996) *Biochemistry 35*, 8986−8994.
52. Bedard, P., and Mabroul, P. A. (1997) *Biochem. Biophys. Res. Commun. 240*, 65−67.
53. Choi, S., Spiro, T. G., Langry, K. C., Smith, K. M., Budd, D. L., LaMar, G. N. (1982) *J. Am. Chem. Soc. 104*, 4345−4351.
54. Spiro, T. G., Li, X. Y. (1988) in *Biological Applications of Raman Spectroscopy* (Spiro T. G., Ed.) Vol 3, pp 1−37, John Wiley & Sons, Inc, New York.
55. Hashimoto, S., Teraoka, J., and Kitagawa, T. (1986) *Proc. Natl. Acad. Sci. U.S.A. 83*, 2417−2421.
56. Smulevich, G., Evangelista-Kirkup, R., English, A., and Spiro, T. G. (1986) *Biochemistry 25*, 4426−4431.
57. Smulevich, G., Dasgupta, S., English, A., and Spiro, T. G. (1986) *Biochim. Biophys. Acta 873*, 88−91.
58. Smulevich, G., Neri, F., Williamsen, O., Choudhury, K., Marzocchi, M. P., and Poulos, T. L. (1995) *Biochemistry 34*, 13485−13490.
59. Smulevich G., Neri, F., Marzocchi, M. P., and Welinder, K. G. (1996) *Biochemistry 35*, 10576−10585.
60. Smulevich, G. (1998) *Biospectroscopy 4*, S3−S17.
61. Strittmatter, P., and Velick, S. F. (1956) *J. Biol. Chem. 221*, 253−264.
62. Yonetani, T., Wilson, D. F., and Seamonds, B. (1966) *J. Biol. Chem. 241*, 5347−5352.
63. Neri, F., Indiani, C., Baldi, B., Vind, J., Welinder, K. G., and Smulevich, G. (1999) *Biochemistry 38*, 7819−7827.
64. Yoshimura, T., and Ozaki, T. (1984) *Arch. Biochem. Biophys. 230*, 466−482.
65. Williams, R. J. P. (1951) *Chem. Rev. 56*, 299−328.
66. George, P., and Hanania, G. (1952) *Biochem. J. 52*, 517−523.
67. Keilin, D., and Hartree, E. F. (1951) *Biochem J. 49*, 88−97.
68. Neri, F., Indiani, C., Welinder, K. G., and Smulevich, G. (1998) *Eur. J. Biochem. 251*, 830−838.
69. Palanappian, V., and Terner, J. (1989) *J. Biol. Chem. 264*, 16046−16053.
70. Neri, F., Kok, D., Miller, M. A., and Smulevich, G. (1997) *Biochemistry 36*, 8947−8953.
71. Erman, J. E. (1974) *Biochemistry 13*, 34−39.
72. DeLauder, S. F., Mauro, J. M., Poulos, T. L., Williams, J. C., and Schwarz, F. P. (1994) *Biochem. J. 302*, 437−442.
73. Yonetani, T., and Anni, H. (1987) *J. Biol. Chem. 262*, 9547−9554.
74. Smulevich, G., Mantini, A. R., English, A. M., and Mauro, J. M. (1989) *Biochemistry 28*, 5058−5064.
75. Patterson, W. R., Poulos, T. L., and Goodin, D. B. (1995) *Biochemistry 34*, 4342−4345.
76. Howes, B. D., Feis, A., Indiani, C., Marzocchi, M. P., Smulevich, G. (2000) *J. Biol. Inorg. Chem. 5*, 227−235.
77. Palmer, G. (1985) *Biochem. Soc. Trans. 13*, 548−560.
78. Dou, Y., Admiraal, S. J., Ikeda-Saito, M., Krzywda, S., Wilkinson, A. J., Li, T., Olson, J. S., Prince, R. C., Pickering, I. J., and George, G. N. (1995) *J. Biol. Chem. 270*, 15993−16001.
79. Hederstedt, L., Andersson, K. K. (1986) *J. Bacteriol. 167*, 735−739.
80. Friden, H., Cheesman, M. R., Hederstedt, L., Andersson, K. K., and Thomson, A. J. (1990) *Biochim. Biophys. Acta 1041*, 207−215.
81. Gadsby, P. M. A., and Thomson, A. J. (1990) *J. Am. Chem. Soc. 112*, 5003−5011.
82. Loewen, P. C., Triggs, B. L., George, C. S., and Hrabarchuk, B. E. (1985) *J. Bacteriol. 162*, 661−667.
83. Magliozzo, R. S., and Marcinkeviciene, J. A. (1996) *J. Am. Chem. Soc. 118*, 11303−11304.

BI0006870